[Article ID]1000-9035(2024)01-081-05
DOI:10.13563/j.cnki.jmolsci.2023.14.011

Study of the evolved behavior of inorganic ammonia molecules inside nanopores

NIU Yanhui[1], YU Wenbin[2], YANG Shuguang[2], WAN Quan*[,2]
1. School of Chemistry and Materials Science, Guizhou Education University, Guiyang 550018, China;
2. State Key Laboratory of Ore Deposit Geochemistry, Institute of Geochemistry, Chinese Academy of Sciences, Guiyang 550081, China

Abstract: This study investigated the effects of the length of long-chain alkyl bromides C_nTAB (n=12, 16) on the structure and properties of the materials. The analysis showed that the size of the nanopores had a significant effect on the escape behavior of ammonia molecules, and the final escape temperature of ammonia molecules within the nanopores increased with decreasing nanopore diameter. For a nanopore of 3.2 nm, the escape temperature can reach 250 ℃. These findings provide data support for the thermal stability of small inorganic molecules in nanopores and inform the energy storage mechanisms of nanoporous materials. These insights are crucial for understanding the thermal stability of inorganic small molecules in nanopores and the energy storage mechanism of nanoporous materials.
Keywords: ammonia; evolved behavior; nanopores

1 Introduction

Renewable energy is a clean and low-carbon source of energy that plays a crucial role in improving our energy structure, protecting the environment, combating climate change, and promoting sustainable economic and social development. While the recycling of renewable energy sources is essential in reducing greenhouse gas emissions, most renewable energy sources are intermittent and require energy storage. Hydrogen and hydrogen carriers are the only viable options for indirect energy storage. However, since hydrogen is difficult to store and transport, hydrogen carriers are proposed for hydrogen storage and transport [1-3]. Ammonia (NH_3) is a clean, high-energy-density hydrogen energy carrier [4-7] that is widely available. It is also an essential chemical raw material and a potential carbon-free fuel energy [8], while porous zeolite is an important adsorbent material [9-10] for ammonia storage gas. Ammonia is also an alkaline ligand commonly used as a molecular probe to study the acidity of hydroxyl groups in oxides, zeolites, and zeolite-like materials. The interaction between the nanopore acid site and the alkaline ligand is reflected in the thermal behavior[11]. Therefore, the structural properties of nanopores are crucial indicators of adsorbent [12].

Nanopores are commonly present in the earth's environment, and both organic and inorganic small molecules can be adsorbed within them. The properties of these molecules can be affected by the active site on the nanopore surface, as well as by the physical and chemical properties of the restricted molecules in the nanopores [13]. While zeolite materials are widely used as adsorbents, deodorants, and desiccants, the influence of nanopore structure features has rarely been discussed [14], and the changes in nanopore structure directly control the escape behavior of inorganic small molecules, affecting the storage capacity of small molecules and their interaction mechanisms.

This paper aims to examine the behavior of ammonia gas molecules escaping through a nanopore. For this purpose, high-purity nanopore silica has been selected as the research object. The study utilizes TG (STA)-FTIR experimental technology to investigate the interaction between ammonia and the limited nano space interface. The change in nanopore size is also studied to control and regulate the mechanism of ammonia molecule escape behavior. The physicochemical properties of ammonia material in the nanopore are closely related to the size effect and surface effect of the nanopore. This study has laid a good foundation for further understanding of the adsorption of inorganic small molecules in solution.

2 Experiment

2.1 Reagents and instruments

The experiment used ammonia with a concentration of 25% to 28% (GR) and other reagents with a purity of 99%. All the reagents were bought from Shanghai Aladdin Biochemical Tech-

Received: 2023-04-02
*Corresponding author.
E-mail address: wanquan@vip.gyig.ac.cn(WAN Quan)

nology Co., LTD. Automatic gas adsorption meter (Autosorb-iQ2-MP, Quantachrome), Organic element analyzer (Elementar Vario MACRO cube, Germany), Infrared spectrometer (Bruker Vertex 70, Germany). Ultrapure water (Millipore/Synergy, France, Resistivity 18.2 MΩ·cm).

2.2 Preparation of nanopore silica

The synthesis of nanopore silica was carried out at 27 ℃ under alkaline conditions, tetraethyl silate was used as the silicon source, and the template agent used in this study was the alkyltrimethylammonium bromide surfactant $C_nH_{2n+1}N^+(CH_3)_3Br^-$ (C_nTAB, $n=12,16$). The samples were then crystallized at 105 ℃ for 18 d, filtered, washed to neutral, and dried at room temperature. After heating the samples to 550 ℃ at a rate of 1 ℃ per minute under an empty atmosphere, the surfactant was removed by roasting for 6 h, resulting in the synthesis of two simulated mineral nanopore samples[15-16] with different pore sizes, namely NPS-1 and NPS-2 (NPS stands for "nanoporous silica"). The series of samples obtained had a uniform pore size distribution, a large specific surface area, and good stability in water.

2.3 Characterization method of nanoporous silica

An Automatic Gas Adsorption Instrument was used to conduct the N_2 (77 K) adsorption experiment. The N_2 purity was 99.999%, and the cross-sectional area was measured to be 0.162 nm^2. The test pressure range (p/p_0) was 10^6 to 0.99. Before testing the nanopore sample, it was kept at 200 ℃ for 20 h. The BET model was used to calculate the specific surface area, and the NLDFT model was used to calculate the diameter and volume of the nanopores.

The Organic Element Analyzer examined the C and N elements in the given samples. Each test required weighing 20 to 50 mg of powdered samples, and each sample was tested twice. The average value of the two tests was taken as the final result for analysis.

The sample was analyzed using Attenuated Total Reflection Infrared spectroscopy (ATR-IR) with a range of 4 000 to 400 cm^{-1}, a resolution of 4 cm^{-1}, and a scanning time of 16.

The escape gas analysis (EGA, Evolved Gas Analysis) is the test of Thermogravimetric Analysis coupled with Fourier Transform Infrared Spectroscopy (TG-FTIR) in an air atmosphere. Samples weighing between 5 to 10 mg are used for the analysis. The heating rate is set to 1 ℃·min^{-1} over a temperature range of 40 ℃ to 550 ℃. During the process, as gas is released due to volatilization, condensation, and combustion, the sample temperature is controlled by a Differential Thermal Analyzer. The released gas is then sent to the infrared gas pool for Infrared Spectrometer. This analysis helps to determine the composition and content of the escaped gas.

3 results and discussion

3.1 Structural analysis of the nanoporous silica

3.1.1 Analysis of the Infrared spectrum

Figure 1 displays the FTIR spectrum diagrams of nanoporous silica that was dried at 30 ℃ and calcined at 550 ℃, respectively. As can be seen from Figure 1, the hydroxyl group (—OH) stretching vibration peak of physically adsorbed water and the surface of nanoporous silica at 3 440 cm^{-1}, the isolated ≡Si—OH stretching vibration peak appears at 3 748 cm^{-1}[17], and the —OH bending vibration peak of physically adsorbed water molecules of nanoporous silica is at 1 640 cm^{-1}. Additionally, the three characteristic peaks of the nanopore silica skeleton[18] are the antisymmetric stretching vibration peak of Si—O—Si at 1 041 cm^{-1}, the symmetric stretching vibration peak of Si—O—Si at 786 cm^{-1}, and the bending vibration peak of Si—O—Si at 440 cm^{-1}.

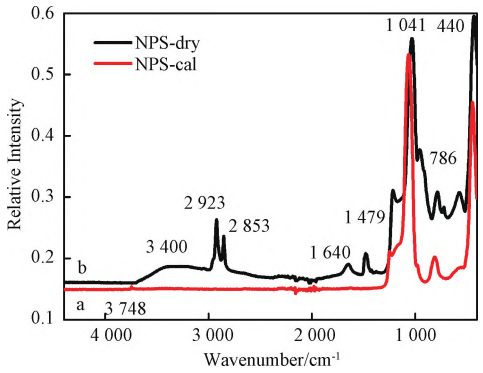

Figure 1 IR spectra of calcined and uncalcined NPS

Upon analysis of curves a and b, it was observed that the characteristic CTAB peak appears in the FT-IR spectrum of uncalcined nanoporous silica. The N—C bending vibration peak is located at 1 479 cm^{-1}, the C—H stretching vibration peak of the —CH_2 group is located at 2 853 cm^{-1}, and the C—H stretching vibration peak of the —CH_3 group[19] is located at 2 923 cm^{-1}. However, in curve b, no characteristic peak of CTAB was observed. The results of organic element analysis indicated that the nitrogen content was between 0.15% and 0.33%, and the carbon content was between 0.03 and 0.05% (See Table 1). These findings suggest that the organic template agent in the nanopore silica, which was calcined at 550 ℃ after heat treatment, had been removed.

3.1.2 The N_2 adsorption-desorption isotherm analysis

The N_2 physical adsorption method is widely used for nanopore material characterization. This method is considered to be one of the most effective ways to determine the specific surface area, pore volume, pore size distribution, and some material surface properties. The automatic gas adsorption instrument can provide all this information, as demonstrated in Table 1.

The size of pores in nanopore silica can be adjusted by altering the length of the hydrophobic group in the surfactant. To ensure uniform pore size distribution and control pore size, a surfactant known as $C_nH_{2n+1}N(CH_3)_3Br$ (where $n=12$, 16) was employed. The subsequent step involves examining how ammonia behaves in the nanoporous silica.

Figure 2a displays the nanoporous silica type Ⅳ isotherm at a temperature of 77 K[20]. This characteristic is commonly observed in mesoporous (2 to 50 nm) materials, where there is a sudden rise in adsorption due to capillary condensation. The adsorption capacity displayed a linear increase in the low-pressure region, indicating the formation of a N_2 monolayer on the pore wall. The steep increase in adsorption capacity during the capillary condensation segment further confirms the uniformity of adsorbed isotherm type of nanoporous materials.

The research performed demonstrated that the adsorption capacity of N_2 on the pore surface increased linearly in the low-pressure section. This suggests that a monolayer of N_2 is present on the pore wall. Furthermore, the capillary condensation segment showed a steeper change in the adsorption capacity, indicating a more uniform pore size distribution. In the high-pressure zone, the sample entered an extended stationary phase, indicating that multilayer adsorption continued on the pore surface. Thus, it can be inferred that the adsorption process is physical and is affected by the size of the pore. Additionally, chemical adsorption occurs only at the chemical active site and is not dependent on the size of the pore[21]. These findings underscore the importance of understanding the adsorption process for N_2 and can help to design more effective separation and purification processes.

Based on the N_2 adsorption-desorption isotherm, the specific surface area and aperture analysis results of BET and DFT models are shown in Figure 2b. It is found that it is a nanopore with different pore volumes with large specific surface area and uniform pore size distribution. Nanopores with uniform aperture were also confirmed on Transmission Electron Micrographs (see Figure 3).

3.2 The escape behavior of ammonia in the nanopore

The results of analyzing the mixture of NPS-1 and NPS-2 with ammonia using Thermogravimetric method are shown in Figure 4c and 4d, respectively. The DSC endothermic peaks at 199 ℃ and 191 ℃, respectively, indicate the decomposition of

Table 1 Structural characteristic parameter of the NPS samples

Sample	Surfactant	S_{BET}/($m^2 \cdot g^{-1}$)	D_{DFT}/nm	V_{DFT}/($cm^3 \cdot g^{-1}$)	x(N)/%	x(C)/%	x(H)/%
NPS-1	C_{12}TAB	842	3.2	0.5	0.15	0.03	0.69
NPS-2	C_{16}TAB	882	4.1	0.8	0.22	0.03	0.60

Note: NPS-1 & NPS-2 synthesized from C_{12}TAB & C_{16}TAB, respectively. Specific surface area calculated with BET; pore size/volume with NLDFT; nitrogen, carbon and hydrogen percentages measured with organic element analyzer.

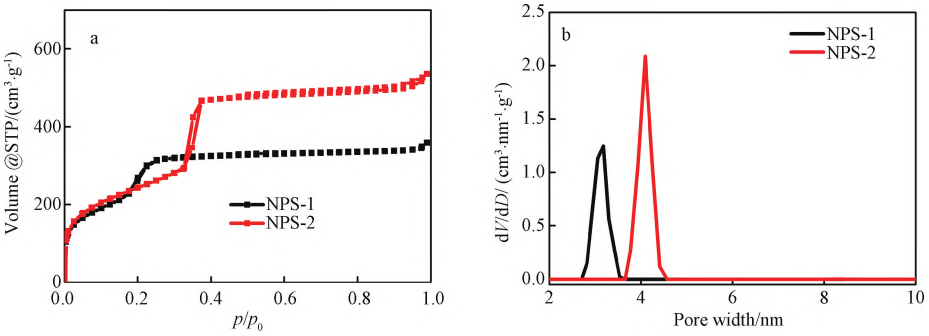

Figure 2 N_2 adsorption/desorption isotherm (a) and pore size distribution of NPS (b)

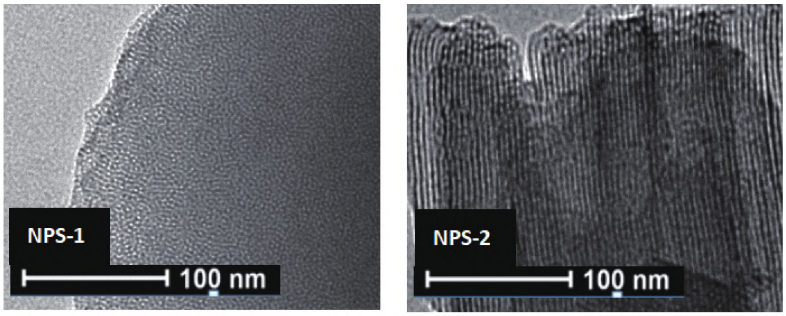

Figure 3 TEM images of NPS-1 and NPS-2

ammonia and water. The DSC peak shifts towards a lower temperature as the pore size increases. The escape temperature of the ammonia gas in the nanopore also increases with the decrease of the pore size (See Figures 4e and 4f). The escape temperature can reach 250 ℃ when the pore size is 3.2 nm (See Figure 4e). There are several forms of ammonia present in the nanopores, such as NH_4^+, OH^-, NH_3, H_2O, and hydrogen bonds. The optimal escape temperature for ammonia is 176 ℃ and 133 ℃ for the respective sizes of pores (as shown in Figure 4e and 4f) and decreases with an increase in pore size. The interaction between ammonia molecules and the wall of the nanopore is intensified, and the confinement within the nanopore makes it difficult for the ammonia gas to escape.

As the temperature rises, ammonia undergoes decomposition to form ammonia and water, which helps in shifting the equilibrium to the right. The formation of hydrogen bonds and nano-confinement result in an increase in the escape temperature of ammonia gas. The chemical reaction can be represented as:

$$NH_4^+ + OH^- \rightleftharpoons NH_3 \cdot H_2O \rightleftharpoons NH_3 + H_2O. \quad (1)$$

Something extraordinary has been revealed in Figures 4e and 4f. The Infrared Absorption Spectrum 3D map of escape gas extracted at 176 ℃ and 133 ℃ shows all four vibration modes of ammonia molecules in the spectrum. One can witness symmetric stretching (ν_1) at 3 337 cm^{-1}, symmetric bending (ν_2) at 931 and 966 cm^{-1}, asymmetric stretching (ν_3) at 3 444 cm^{-1}, and asymmetric bending (ν_4) at 1 627 cm^{-1}. These findings from Figures 4e and 4f have opened avenues for further research and discoveries.

It has been observed that ammonia molecules have a higher escape velocity than water molecules, as shown in Figures 4a and 4b. Interestingly, the escape peak of ammonia molecules weakens at around 200 ℃ in the Infrared Absorption Spectrum due to the hydrogen bonding between ammonia and water molecules. Water and ammonia molecules restrict each other, but the hydrogen bonding interaction of water molecules remains strong. However, the interaction between NH_3, H_2O, and the pore wall increases within nano-confinement, raising the escape temperature. Therefore, nanopores are an excellent storage space for ammonia gas.

Understanding the structural features of NPS-1 and NPS-2 from Table 1 is essential for gaining insights into the behavior of ammonia molecules. NPS-2 has a larger specific surface area, pore size, and pore volume than NPS-1. However, the final escape temperature of ammonia molecules in NPS-1, which has a pore size of 3.2 nm, is almost 50 ℃ higher than that of ammonia molecules in NPS-2. Although the specific surface area of NPS-2 is 882 $m^2 \cdot g^{-1}$, more than that of NPS-1, the density of the surface hydroxyl group is reduced. Most ammonia and water molecules are more physisorbed than chemisorbed with the nanopore walls. Therefore, it can be concluded that the nano-confinement effect plays a crucial role in the escape behavior of the ammonia molecules.

4 Conclusions

This paper explores the effect of spatial confinement on ammonia in nanopores and the optimal temperature for inorganic ammonia molecules to escape. The experimental results indicate that the escape temperature of inorganic ammonia molecules in the nanopore can reach 250 ℃, and this temperature increases as the pore size decreases. This research provides a fundamental rationalization basis for the physical adsorption and inter-molecular hydrogen bond mechanism of ammonia storage materials, and direct evidence for the nanopore protection mechanism of inorganic small molecules. It also provides data support for the mech-

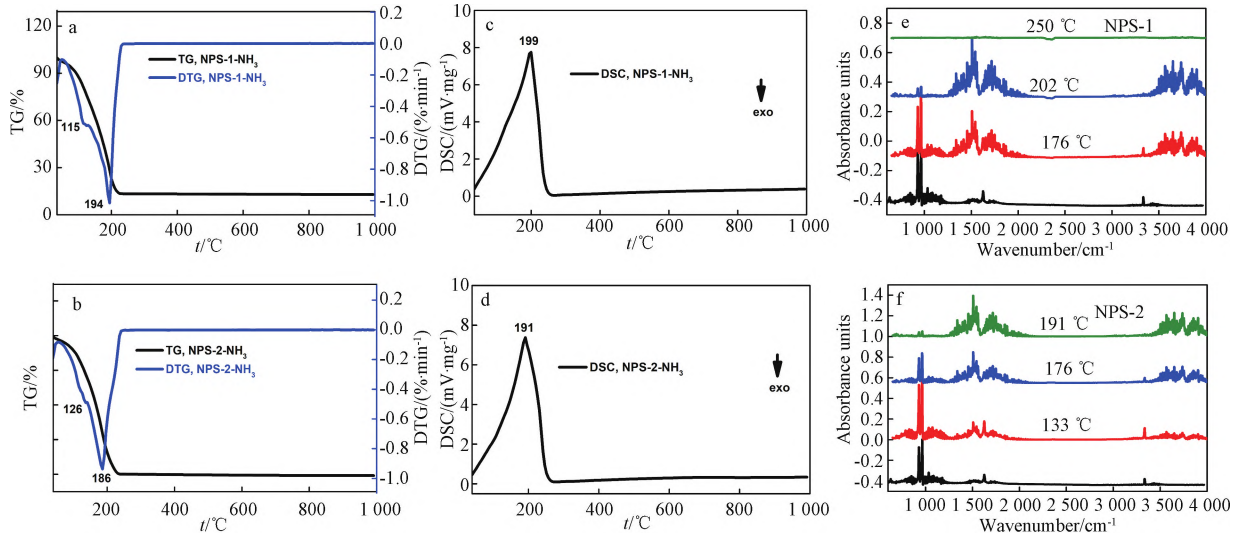

Figure 4 TG/DTG curves (a and b), DSC curves(c and d)and the extracted spectra of evolved gas(e and f)of NPS with ammonia

anism of confinement effect for small molecule adsorption in nanopores and offers new ideas and solutions for applications in fields such as sensors, gas storage, and separation.

Acknowledgement

The project was supported by the Doctoral Program Foundation of Guizhou Education University (2022BS010), the Science Technology Department Foundation of Guizhou Province (QianKeHePingTaiRenCai[2018]5778-10), and the Natural Science Foundation of Department of Education of Guizhou Province (QianJiaoHe KY (2021)021).

Reference

[1] GÖTZ M, LEFEBVRE J, MÖRS F, et al. [J]. Renew Energ, 2016, 85: 1371-1390. DOI: 10.1016/j.renene.2015.07.066.
[2] ROUWENHORST K H R, VAN DER HAM A G J, MUL G, et al. [J]. Renew Sust Energ Rev, 2019, 114: 109339. DOI: 10.1016/j.rser.2019.109339.
[3] GIDDEY S, BADWAL S P S, MUNNINGS C, et al. [J]. ACS Sustainable Chem Eng, 2017, 5(11): 10231-10239. DOI: 10.1021/acssuschemeng.7b02219.
[4] VALERA-MEDINA A, XIAO H, OWEN-JONES M, et al. [J]. Prog Energy Combust Sci, 2018, 69: 63-102. DOI: 10.1016/j.pecs.2018.07.001.
[5] GUO J P, CHEN P. [J]. Chem, 2017, 3(5): 709-712. DOI: 10.1016/j.chempr.2017.10.004.
[6] VALERA-MEDINA A, BANARES-ALCANTARA R. Techno-Economic Challenges of Green Ammonia as an Energy Vector[M]. UK: Academic Press, 2020.
[7] ZHANG L F, FAN Y J, MAO C C, et al. [J]. Inorg Chem Ind, 2023, 55(3): 21-27. DOI: 10.19964/j.issn.1006-4990.2022-0309.
[8] YE L, LO B T W, QU J, et al. [J]. Chem Commun, 2016, 52(16): 3422-3425. DOI: 10.1039/C5CC10476A.
[9] ROUWENHORST K H R, MANI S, LEFFERTS L. [J]. ACS Sustainable Chem Eng, 2022, 10(6): 1994-2000. DOI: 10.1021/acssuschemeng.1c08467.
[10] TAKEUCHI M, TSUKAMOTO T, KONDO A, et al. [J]. Catal Sci Technol, 2015, 5(9): 4587-4593. DOI: 10.1039/C5CY00753D.
[11] ZECCHINA A, MARCHESE L, BORDIGA S, et al. [J]. J Phys Chem B, 1997, 101(48): 10128-10135. DOI: 10.1021/jp9717554.
[12] GORDINA N E, BORISOVA T N, KLYAGINA K S, et al. [J]. Membranes, 2022, 12(2): 147. DOI: 10.3390/membranes12020147.
[13] ZHENG A, LIU S B, DENG F. [J]. Chem Rev, 2017, 117(19): 12475-12531. DOI: 10.1021/acs.chemrev.7b00289.
[14] TAKEUCHI M, TSUKAMOTO T, KONDO A, et al. [J]. J Near Infra Red Spec, 2019, 27(3): 241-249. DOI: 10.1177/0967033519836.
[15] GRÜN M, UNGER K K, MATSUMOTO A, et al. [J]. Micropor Mesopor Mat, 1999, 27(2/3): 207-216. DOI: 10.1016/S1387-1811(98)00255-8.
[16] NIU Y H, YU W B, QIN Z H, et al. [J]. Acta Geochim, 2019, 38: 517-529. DOI: 10.1007/s11631-019-00358-6.
[17] MCCOOL B, MURPHY L, TRIPP C P. [J]. J Colloid Interf Sci, 2006, 295(1): 294-298. DOI: 10.1016/j.jcis.2005.08.010.
[18] ZHU W J. Preparation of MCM-41 Mesoporous Molecular Sieve and Its Adsorption of Heavy Metal Ions[D]. Kunming: Kunming Institute of Technology, 2013.
[19] SARI YILMAZ M, DERE ÖZDEMIR Ö, PIŞKIN S. [J]. Res Chem Intermed, 2015, 41: 199-211. DOI: 10.1007/s11164-013-1182-4.
[20] THOMMES M, KANEKO K, NEIMARK A V, et al. [J]. Pure Appl Chem, 2015, 87(9/10): 1051-1069. DOI: 10.1515/pac-2014-1117.
[21] CHOI S W, BAE H K. [J]. KSCE J Civ Eng, 2014, 18: 1977-1983. DOI: 10.1007/s12205-014-0229-4.

无机氨分子在纳米孔中的逸出行为研究

牛延慧[1],于文彬[2],杨曙光[2],万 泉[*,2]
1. 贵州师范学院化学与材料学院,贵州 贵阳 550018;
2. 中国科学院地球化学研究所矿床地球化学国家重点实验室,贵州 贵阳 550081

[摘 要] 利用长链烷基溴化季铵盐 C_nTAB(n=12,16)模板剂,水热法制备了高纯度纳米孔二氧化硅。采用红外光谱仪、元素分析仪及气体吸附仪对纳米孔二氧化硅的孔结构进行了分析;通过热红联用同步热分析技术(TG(STA)-FTIR)探讨了在2种不同孔尺寸(3.2和4.1 nm)、组成单一且孔径均一的纳米孔中无机氨分子的受热逸出行为。数据结果表明,纳米孔内氨气的最终逸出温度随着孔尺寸的降低而增大,逸出温度可高达250 ℃。研究空间限制效应对纳米孔内氨水逸出行为的影响,不仅为无机小分子在纳米孔中的热稳定性及热运动提供了数据支撑,同时为纳米孔材料氢能载体存储机制提供了参考价值。

[关键词] 氨气;逸出行为;纳米孔